IEEE Access
Multidisciplinary ⁝ Rapid Review ⁝ Open Access Journal

Received February 20, 2022, accepted March 15, 2022, date of publication March 22, 2022, date of current version April 11, 2022.

Digital Object Identifier 10.1109/ACCESS.2022.3161565

Simultaneous User Localization and Identification Using Leaky-Wave Antennas and Backscattering Communications

KYRIAKOS NEOPHYTOU[1], (Student Member, IEEE), MATTHIAS STEEG[2], (Member, IEEE), JONAS TEBART[2], (Student Member, IEEE), ANDREAS STÖHR[2], (Senior Member, IEEE), STAVROS IEZEKIEL[1], (Senior Member, IEEE), AND MARCO A. ANTONIADES[1,3], (Senior Member, IEEE)

[1]Department of Electrical and Computer Engineering, University of Cyprus, 1678 Nicosia, Cyprus
[2]Department of Optoelectronics, University of Duisburg-Essen, 47057 Duisburg, Germany
[3]Department of Electrical, Computer and Biomedical Engineering, Ryerson University, Toronto, ON M5B 2K3, Canada

Corresponding author: Kyriakos Neophytou (kyriakos.neofitou@ucy.ac.cy)

This work was supported in part by the European Network for the High Performance Integrated Microwave Photonics (EUIMWP) Cost Action; in part by the European Regional Development Fund and the Republic of Cyprus through the Research and Innovation Foundation, under the Project INFRASTRUCTURES/1216/0042 (RF-META); and in part by the University Duisburg-Essen through the German Research Foundation (Deutsche Forschungsgemeinschaft) under Grant CRC/TRR 196 MARIE project C07.

ABSTRACT High-speed detection and identification of mobile terminals located in the vicinity of highly directive base stations is essential for future mm-wave communication systems. We propose a novel optoelectronic frequency modulated continuous wave (FMCW) radar system for detection, localization and identification of multiple mobile terminals. The simultaneous localization and identification of multiple mobile terminals is achieved by using frequency scanning mm-wave leaky-wave antennas (LWAs) and backscattering communications. LWAs provide RF-based beam steering for estimating the direction of arrival of the echoes using a FMCW radar signal. Additionally, the implementation of backscattering technology in the mobile terminals allows the identification of users. Hence, simultaneous user localization and identification without the use of any complicated radar signal post-processing algorithms is possible. Finally, the introduced modulated backscattering reflection shifts the signals of the targets at higher frequencies, which exhibit lower noise floor and thus have higher signal to noise ratio (SNR).

INDEX TERMS Leaky-wave antennas, backscattering communications, radio frequency identification, 5G, automotive radar, localization, identification, microwave photonics.

I. INTRODUCTION

The thousand-fold increase in mobile data traffic from 5G networks will be achieved by moving to a wider RF bandwidth, higher spectral efficiency and reduced cell sizes [1]–[3]. In particular, the large bandwidth of about 8 GHz available at mm-wave bands (e.g. the 26 GHz band) is seen as an enabler for 5G applications [2]–[4]. To mitigate the high free-space path loss, directive and multibeam antennas with beam steering capabilities are required; LWAs operating at mm-waves can enable beam steering via frequency scanning, thus also offering the generation of multiple beams. Moreover, LWAs only require a single RF feeding port and no additional control signals and can still provide high directivities and radiation efficiencies [5], advantages which were used in [6] to demonstrate a fiber-wireless communication system for multiple users.

Since the end users are mobile, it is necessary to localize and identify the mobile terminals (MTs) for mm-wave mobile access. This has led to interest in mm-wave direction-of-arrival (DoA) estimation to enable the localization of MTs and the utilization of beam steering antennas [7]. A high-gain link between the base station and the MTs can be achieved by steering the beams of the LWA towards the localized and identified users. However, existing approaches require immense post processing algorithms which increase the latency of the localization and identification [7]–[17]. In [10], a phased array is used to localize and identify RFID tags which leads to spurious results due to the multipath effect, thus requiring a dedicated post-processing algorithm

The associate editor coordinating the review of this manuscript and approving it for publication was Muguang Wang.

which increases the latency and the estimation time. Other solutions do not enable the simultaneous localization and identification of the radar echoes and thus they cannot be implemented in 5G communication systems [11], [12], while machine learning-based approaches require a large amount of training data and thus cannot be implemented in random and unknown scenarios [13], [14]. Additionally, state-of-the-art solutions such as UWB and WiFi localization [15]–[17] provide precise user localization and identification, but require at least three transceivers (for 2D localization) placed at different locations. This results in an increased deployment cost. In [18], 3D target localization was achieved using a photonic FMCW radar with two linearly polarized microstrip LWAs operating at 26 and 28 GHz bands. Radar systems are well established for ranging, detection, localization, and speed estimations, and the unique properties of LWAs are frequently used as radar antennas due to their beam steering capabilities [19], [20].

In this work, we propose the implementation of backscattering communications [21]–[23] and a photonically-enabled frequency-modulated continuous-wave (FMCW) radar with LWAs in order to simultaneously identify and localize the MTs. Backscattering MTs (BMTs) can modulate and reflect the mm-wave signals sent from the photonic FMCW radar. Hence, the photonically enabled FMCW radar is able to localize and identify the MTs by receiving and de-modulating the backscattered mm-wave signals. Due to the frequency scanning nature of the LWAs, the carrier frequency of the modulated mm-wave signals enables DoA estimation and ranging of the BMTs. In addition, the modulation introduced by the backscattering technique enables the identification of the BMTs. Hence by incorporating LWAs and backscattering communication, the BMTs can be localized and identified simultaneously without the need for dedicated radar signal post-processing algorithms. Thus, the latency of the detection processing is reduced.

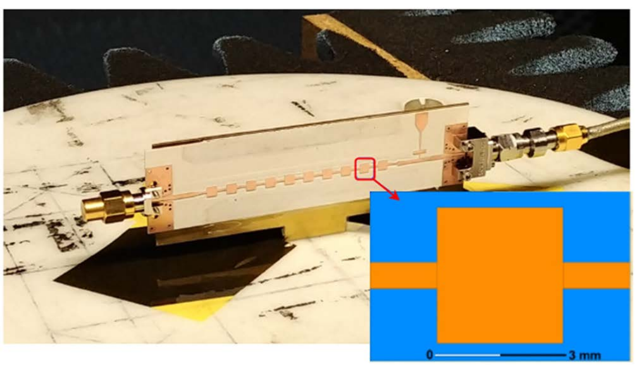

FIGURE 1. Fabricated LWA antenna at 28 GHz, consisting of 10 series-fed microstrip patches (unit cells). Inset diagram showing a single patch unit cell. The length of each unit cell is 5.95 mm, the patch has a width of 2.9 mm and a length of 2.85 mm, and the two microstrip lines before and after the microstrip patches have a width of 0.5 mm and a length of 1.55 mm.

The paper is divided as follows. In Section II the LWA design is presented. Then in Chapter III the architecture of the FMCW radar system is shown. In Chapter IV, the backscattering communication technology, and the backscattering mobile terminals (BMTs) are described. Finally, in Chapter V, experimental results are presented that demonstrate the capability of simultaneous localization and identification of the BMT. Finally, the conclusions of this work are presented in Chapter VI.

II. LEAKY-WAVE ANTENNA DESIGN

LWAs are traveling-wave antennas that are implemented in a guiding structure [24], [25]. These antennas can produce a radiating beam at an angle dictated by the frequency, with a directivity limited by the size of the structure itself [24]. Thus, they possess inherent multi beam capabilities by feeding to the antenna a multi band signal. Unlike phased arrays, LWAs do not require any complicated feeding network and they can be realized with only one input port; this simplicity makes them attractive for high frequency and large-scale applications [24]. When operated in the appropriate region, LWAs radiate a guided fast wave, while propagating along the guiding structure. The phase constant of the guided fast wave controls the radiation angle, and the attenuation constant of the wave determines the efficiency [26]. In principle, when the phase progression between the unit cells is positive the LWA radiates in the forward direction, and when the phase progression between the unit cells is negative, in the backward direction. The radiation angle can be calculated using [24]:

$$\theta = sin^{-1}\left(\frac{\Phi_0}{kd}\right) \tag{1}$$

where, k is the wavenumber, d is the unit cell length, θ the radiation angle, and Φ_0 is the progressive phase shift between each unit cell. Therefore, the radiation angle of the LWA can be selected by appropriately adjusting the phase shift between the unit cells of the LWA. The phase progression is dependent on the frequency of operation and therefore the main beam of the LWA can be steered by varying the frequency.

Radiation in the broadside direction is attained when the phase progression between the unit cells is zero. A careful design must be carried out to achieve broadside radiation, due to the stop band behavior of such periodic structures at the zero-phase progression [27]–[32]. Here, asymmetry of the LWA's unit cell is implemented so that the stop band is reduced and the gain of the LWA around broadside is increased [32].

The LWA operating at the 26 and 28 GHz bands, from 24 GHz to 33 GHz (Fig. 1) is based on the antenna presented in [32]. It is designed to cover both 26 and 28 GHz mm-wave bands, as used in 5G and mm-wave radar applications. As shown in Fig. 1, the LWA consists of a periodic arrangement of series-fed microstrip patches. The length of the unit cells are equal to a guided wavelength at 28 GHz. The unit cell design includes three microstrip lines in series, two high impedance lines with a width of 0.5 mm and a length of 1.55 mm, and one low impedance line (patch) in between the two high impedance lines with a width of 2.9 mm and a length of 2.85 mm. The unit-cell design of the LWA is illustrated in the inset of Fig. 1 and is optimized for broadside radiation as well as linear steering through the broadside direction. The main radiating elements of the LWA are the microstrip patches, and thus the radiation efficiency is highly proportional to the number of the unit cells. By increasing the number of unit cells, a higher percentage of the guided wave can leak out, thus increasing the radiation efficiency and gain of the LWA. On the other hand, as the number of unit cells increases, the overall size of the LWA increases and for some applications where there are size restrictions this is not optimal. In the case of radar applications, by increasing the size of the LWA the resolution can be increased. Therefore, there is a trade-off between size and resolution. The fabricated LWA with 10 unit-cells is depicted in Fig. 1.

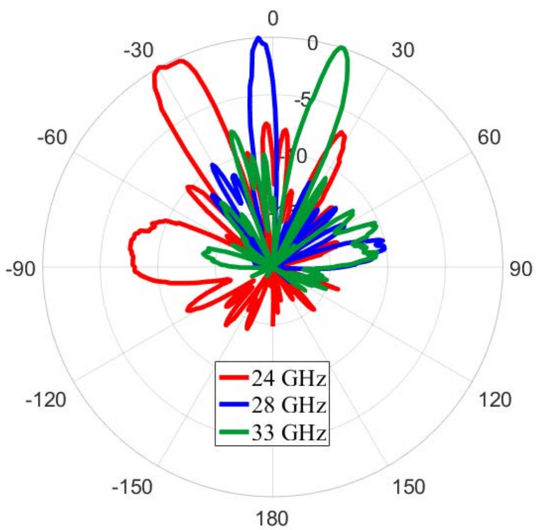

FIGURE 2. Measured normalized LWA radiation patterns for 24, 28 and 33 GHz, demonstrating beam steering capabilities in the H-plane.

The measured H-plane radiation patterns at 23, 28 and 33 GHz are plotted in Fig. 2. It can be seen that the LWA radiates at broadside at around 28 GHz and is steered from -29.5° at 24 GHz to $+18^\circ$ at 33 GHz. The radiation pattern in the E-plane is a fan beam, since the LWA is one-dimensional. Wide-angle beam steering is achieved by using a laminate with a high dielectric constant [33]. Additionally, as seen in Fig. 3 the gain is maintained between 10 and 15 dBi throughout the frequency range of 23 to 33 GHz. It can be seen that the gain is maintained throughout this frequency range, and especially around the 28 GHz broadside frequency, effectively demonstrating that the asymmetry of the LWA unit cells helps to maintain a closed stopband for the periodic structure [32].

Finally, Fig. 4 shows the obtained main beam angles over the operational frequency range of the LWA. The LWA is capable of covering 48° over a bandwidth of 10 GHz. The correlation between the radiation angle and frequency is significantly important for our proposed work, since it can be

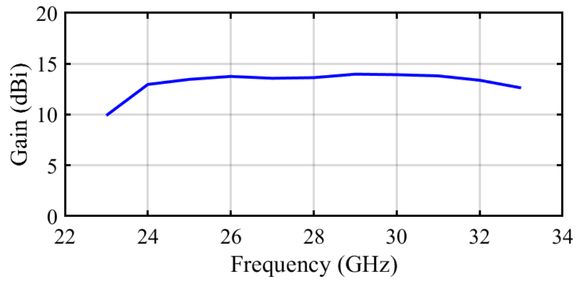

FIGURE 3. Measured gain of the LWA antenna as a function of frequency.

used to identify the direction of arrival of the MBTs echoes. Due to the outlined beam steering capabilities of the LWA, the applied radar FMCW signal with a bandwidth of 10 GHz from 23 GHz to 33 GHz steers the beam along the coverage angle. This enables the estimation of the DoA and distance simultaneously, and thus the localization of the BMTs. In the following section this process will be explained in detail.

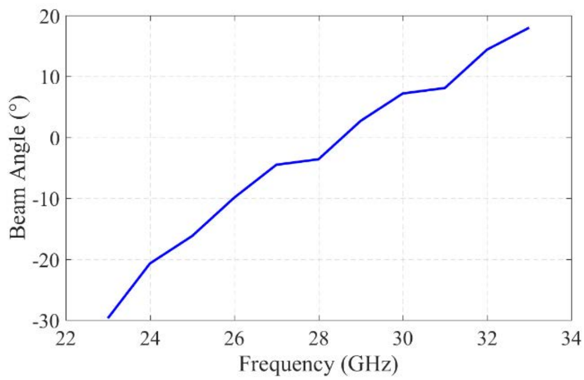

FIGURE 4. Beam steering of the main radiated beam with frequency.

III. FMCW RADAR SYSTEM

The radar system is based on the well-known FMCW technique. FMCW radars use a swept frequency signal to achieve accurate ranging and avoid short, high energy pulses [34], [35]. A periodic FMCW signal can determine the time of flight and therefore the range of the radar system target by comparing the instantaneous RF of the transmitted and the received signal. Therefore, the Time of Flight (*ToF*) can be determined by the beat frequency [32]:

$$\frac{f_{\mathrm{IF,echo}}}{ToF} = \frac{B}{T} \tag{2}$$

where $f_{\mathrm{IF,echo}}$ is the beat frequency of the target, B is the bandwidth and T the period of the FMCW signal. Knowing the *ToF* of the signal from the transmitting (Tx) to the receiving (Rx) antenna, and using the speed of light, c, as the speed of the signal in air, the distance can be estimated using [36]:

$$R = \frac{ToF}{2} c \tag{3}$$

The ranging capabilities of an FMCW radar can be improved by isolating the Rx and Tx antennas, by achieving line of sight to the target, and if no multi-path reflection occurs. By using high-gain antennas, the above requirements can be ensured. Additionally, the radar Equation (4) below further highlights the importance of both Tx and Rx antenna gains (G_t, G_r) since they can directly increase the received power (P_r) as shown below [36]:

$$P_r = \frac{P_t G_r G_t \lambda^2 \sigma}{(4\pi)^3 r^4} \tag{4}$$

Here, P_t is the transmitted power, P_r is the received power, G_t and G_r is the transmitter and receiver gain respectively, λ is the wavelength of the transmitted signal, σ is the target radar cross section area, and r is the distance of the target. In addition to the receiver and transmitter antenna gains, also important to the received power are the target's cross section and distance. The received power decreases with the square of the distance and increases with the square of the target's cross section.

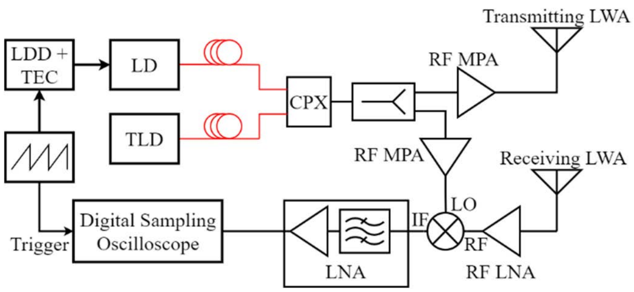

FIGURE 5. FMCW radar system with frequency steerable transmit and receive LWAs that were utilized in this work. LDD: laser diode driver, LD: laser diode, TLD: tunable laser diode, CPX: coherent photonic mixer, MPA: microwave power amplifier, LNA: low noise amplifier.

The proposed architecture for the FMCW radar system with frequency steerable transmit and receive LWAs is shown in Fig. 5. The radar system uses the steerable LWAs presented in Section II. While the FMCW signal is swept over the RF bandwidth, the beam of the transmit LWA is steered over the full coverage angle. The RF FMCW signal is generated by using a CW laser diode (LD), a tunable laser diode (TLD) and a coherent photonic mixer (CPX) as depicted in Fig. 5. The system is highly flexible and a variety of FMCW signals can be realized.

The detection process is as follows: The RF FMCW is generated and transmitted into free space using the transmitting LWA which is simultaneously steered over the coverage angle. Objects within this coverage angle reflect part of the radar signal to the receiving LWA, which receives it at the same angle at which it was transmitted to the object due to antenna reciprocity. The received signal, which contains the radar echoes, is then downconverted by the RF mixer, with the reference FMCW signal acting as a local oscillator. The downconverted IF radar signal is then amplified and captured by a sampling oscilloscope. The captured time domain signal contains the whole period of the FMCW signal. Consequently, while the beat signal contains the distance of the detected object, the time instant of the echo contains the direction of arrival of the object since each time index corresponds to a specific frequency. An example of a downconverted signal is shown in Fig. 6. The time domain form of the downconverter signal is shown in Fig. 6 (a), the target can be distinguished from the rest of the signal from its higher frequency and voltage variation. The data can be evaluated by plotting the FFT weights (Fig. 6 (b)) of the data over their frequencies and the time index by applying a sliding Hanning window FFT over the sampled IF waveform. Therefore, distance and DoA can be estimated simultaneously using this FMCW radar system with limited processing power.

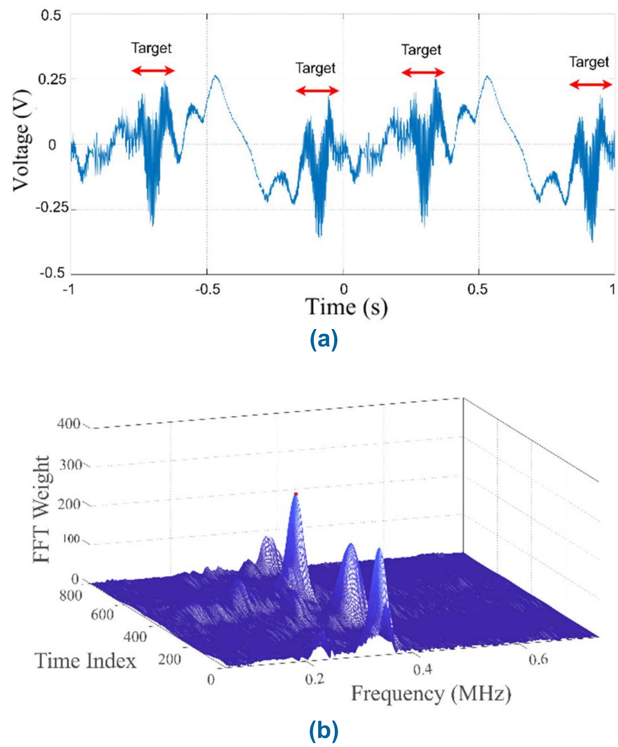

FIGURE 6. Captured waveform of the (a) downconverted signal showing a detected object and (b) its FFT.

In telecommunication systems where the beams should be steered towards the correct BMTs, localization alone is not sufficient, and identification is also required. Combining backscatter communication techniques, identification can be achieved simultaneously without additional processing time. In the following section, backscatter communications will be presented that will enable the identification of the BMTs.

IV. BACKSCATTER COMMUNICATIONS

Backscatter communication techniques are widely used in RFID applications due to their ultra-low power consumption and simplicity [37]–[41]. Here, backscattering communication is employed in order to identify the BMTs. A pin diode is implemented at the BMT's antenna which enables the modulation and reflection of the received signals. This is achieved by switching between open circuit and short

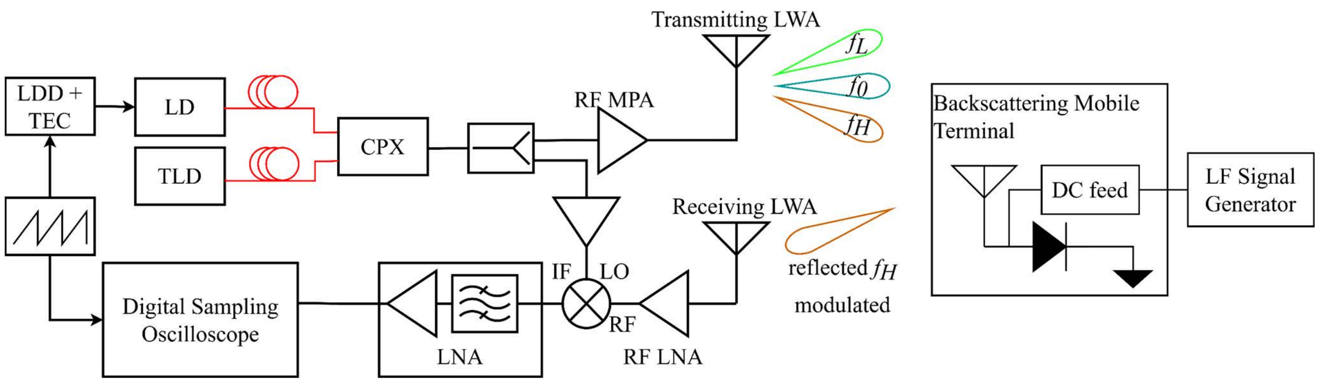

FIGURE 7. Backscatter radar measurements system including the FMCW radar system with frequency steerable transmit and receive LWAs (left side) and the backscattering mobile terminal (right side). The BMT includes an antenna, a Schottky diode, a DC feed and a LF signal generator that switches ON and OFF the Schottky diode.

circuit conditions. The ID of the BMTs is defined in the modulation frequency. For a more advanced ID, an FM code can be implemented with similar effort.

A photonic FMCW radar system that implements backscattering mobile terminals is shown in Fig. 7, where the radar is used to generate and transmit the radio signal and a BMT is used to receive, modulate and reflect the radio signal back to the reader. The BMT can implement two different states that exhibit different impedances and therefore reflect the received signal differently. By periodically switching between these two states, the received signal is modulated. Therefore, the BMT does not require any dedicated RF signal source and its complexity and size can be reduced significantly. In the context of this work, where mm-wave frequencies are to be used, there will be significant free-space path loss (FSPL) and thus the link budget should be evaluated. In the case illustrated in Fig. 7, the communication link roundtrip path loss will limit the maximum achievable distance [37]. This is a bi-static, collocated backscatter link and the link budget for the received modulated backscatter power P_{r} is [37]

$$P_r = \frac{P_t G_{t,r}^2 G_{BMT}^2 \lambda^4 X^2 M}{(4\pi r)^4 B^2 F_a}, \tag{5}$$

where X is the polarization mismatch, M is the modulator factor, B is the path-blockage loss, G_{BMT} is the gain of the BMT's antenna and F_{a} is the fade margin. Hence, to increase the received power, P_{t}, G_{r}, G_{t}, G_{BMT} and M should be increased and B and F_{a} should be decreased. Equation (5) is a slight variation of the radar equation (4), where scattered power decreases by r^4. Here, P_{t} is limited and finite due to the power constraints of the system. G_{r} and G_{t} can be increased by implementing directional antennas at the radar. In our case, two LWAs are used, one as a transmitter and another as a receiver. LWA gain can be increased by increasing their length and number of unit cells. Another important parameter that can be optimized is the modulation factor, M, which is given by

$$\mathrm{M} = \frac{1}{4}|\Gamma_A - \Gamma_B|^2 \tag{6}$$

where, Γ_A and Γ_B are the reflection coefficients of state A and B of the BMT respectively. These two states can be used to code binary "1" and "0". Therefore, the modulation factor is defined as the difference between the load states. The reflection coefficient can be calculated using the following equation [37]:

$$\Gamma = \frac{Z_{L(A,B)} - Z_{ANT}^*}{Z_{L(A,B)} + Z_{ANT}^*} \tag{7}$$

where, $Z_{L(A,B)}$ is the input impedance of the load conditions A and B, and Z_{ANT} is the input impedance of the antenna. This shows that the BMT can control the reflected signal's power and phase by controlling the reflection coefficient Γ. Additionally, by evaluating Equations (6) and (7) we can conclude that the modulation factor is maximized when the two states of the BMT are ideal open-circuit and ideal short-circuit, resulting in $+1$ and -1 reflection coefficients, respectively. In this case, M is maximized and equals unity. Both states will reflect the signal back but with a 180° phase difference, thus binary phase modulation (PM) is realized. In passive backscattering tags, the choice of modulation factor creates a trade-off between design parameters [30]. This is because in ideal open-circuit and short-circuit states, all the power is backscattered, which is not an option for passive devices. Often in RFID and NFC applications a passive backscattering tag should be able to harvest power for its internal analogue blocks and use amplitude-shift-keying (ASK) modulation [41]. In ASK modulation one state is a matched load and the other a short circuit. For the matched load state, the power is absorbed by the passive backscattering tag and during the short circuit state the received power is backscattered, resulting in reflection coefficients of 1 and 0, respectively. The modulation factor, M, of the amplitude modulation will be 1/4, four times smaller than the phase modulation (PM) implementation. As shown in Equation (5) this will reduce the received power P_{R} by a factor of four.

Furthermore, by re-arranging Equation (5) the maximum distance can be calculated for a given radar and backscattering mobile terminal:

$$r = \frac{\lambda}{4\pi}\sqrt{\frac{G_{t,r}G_{BMT}}{B}}\sqrt[4]{\frac{P_t M}{P_r F_a}} \tag{8}$$

Finally, power harvesting is not a requirement since the used BMTs are active devices and are powered by their own battery (see Fig. 7). Therefore, PM was selected due to its maximized modulation factor and improved link budget. Furthermore, the switching between the two states is done with a PIN diode, which requires only minimal power.

V. BACKSCATTERING MOBILE TERMINALS

The BMT consists of an antenna and a switching mechanism that switches between open-circuit and short-circuit states. The switching mechanism was realized using a single PIN diode operating as a single-pole single throw (SPST) switch, as depicted in Fig. 8. The MADP-000907-14020P PIN diode from MACOM™ [42] was selected due to its high switching speeds (which are on the order of a few nanoseconds) and its ultra-low capacitance which allows for operation up to 70 GHz. Additionally, it possesses low insertion loss, high return loss and high isolation. By biasing the diode as shown in Fig. 8, the antenna is short-circuited when the PIN diode is biased, and when the PIN diode is unbiased the antenna is open-circuited. Therefore, a single PIN diode can control the two states of the BMT and enable the modulation of the received signal, as explained in Section IV.

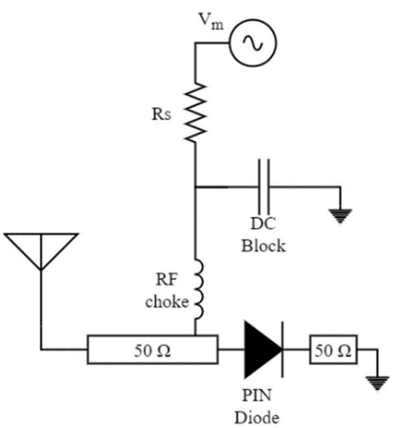

FIGURE 8. BMT circuit design using a SPST switch to implement "1" and "0" states. This includes a single high frequency PIN diode and a biasing circuit.

The antenna of the BMT must be able to cover the operational bandwidth of the LWAs and the radar system described in Sections II and III. Therefore, a horn antenna operating in the 26 GHz band was selected, which can cover a wide bandwidth. The SPST switch (Fig. 8) was realized on a Rogers RT/duroid 5880 substrate with a dielectric constant of 2.2 and a loss tangent of 0.0028. The PIN diode is biased using a DC bias microstrip circuit. The biasing circuitry design is an important part in the design of switching devices. Its main functionality is to provide sufficient biasing voltage and current to the active devices when needed. Additionally, the SPST circuit shown in Fig. 8 consists of an RF choke and DC block. The realized SPST switch circuit can be seen in Fig. 9.

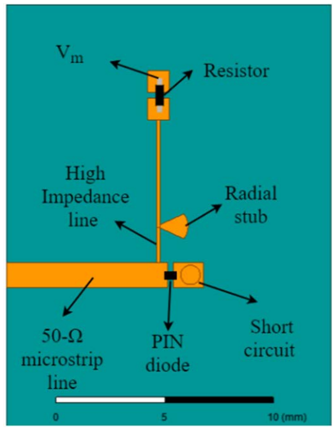

FIGURE 9. Realized microstrip SPST circuit at 28 GHz, implemented on a Rogers RT/duroid 5880 laminate. The details of the single PIN diode and the microstrip biasing network are shown.

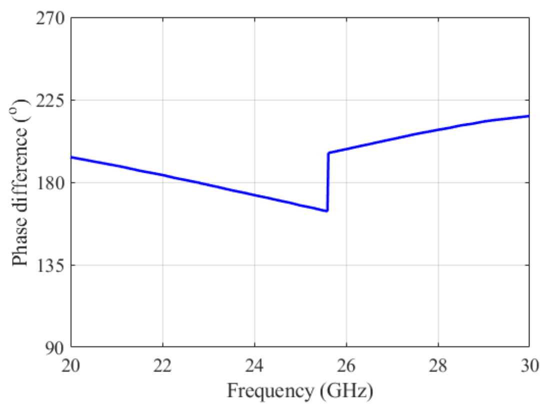

FIGURE 10. Phase difference between the two states of the BMT for short- and open-circuit terminations.

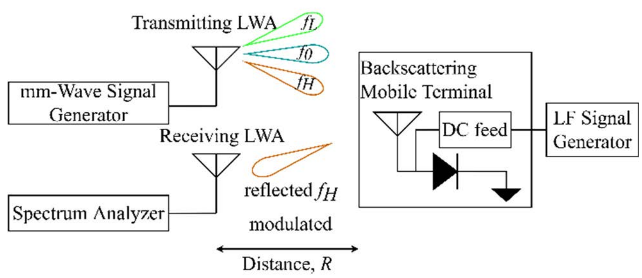

FIGURE 11. Experimental setup for the evaluation of the BMT.

The SPST is implemented on a 50 Ω microstrip line directly after the 50 Ω connector that connects to the horn antenna. The SPST switch is compact and can easily be implemented in standard mobile terminals. Fig. 10 shows the

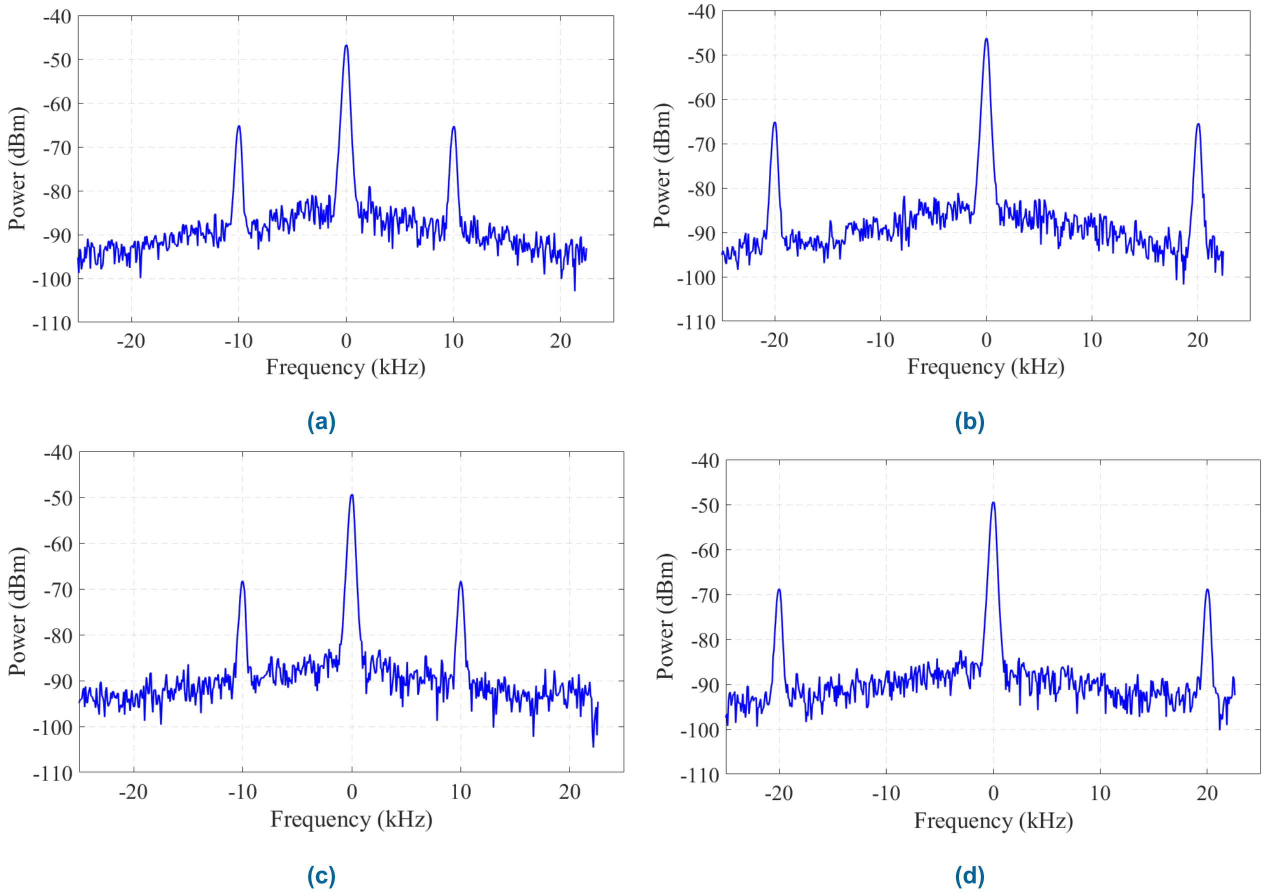

FIGURE 12. Measured backscattered signals, (a) with modulation sidebands $f_m = 10$ kHz at DoA $= -20°$ (f_c is 24 GHz), (b) $f_m = 20$ kHz at DoA $= -20°$ (f_c is 24 GHz), (c) $f_m = 10$ kHz at DoA $= +10°$ (f_c is 31 GHz), and (d) $f_m = 20$ kHz at DoA $= +10°$ (f_c is 31 GHz).

phase difference between the two states of the BMT. It can be seen that this is close to 180° for the required bandwidth of 10 GHz. Having a 180° phase difference between the two states, the modulation factor can be maximized, thus increasing the received power, P_R.

VI. EXPERIMENTAL VERIFICATION OF THE BACKSCATTERING RADAR SYSTEM

First, the correct operation of the BMT was evaluated using the setup illustrated in Fig. 11. The transmitting LWA transmits the signal generated by the mm-wave signal generator into free space at a specific angle based on the frequency of the signal. The BMT is located at the corresponding angle of radiation of the transmitting LWA and it is able to receive the signal with its mm-wave horn antenna. Then, the BMT modulates the phase of the received signal using its SPST switch presented in Section V and reflects it back. The receiving LWA then detects the phase modulated signal, which is measured with an electrical spectrum analyzer. This is a close to the ideal scenario where the modulation can be easily observed and measured, enabling the evaluation of the BMT for all the carrier frequencies, angles of arrival and modulation frequencies. Numerous measurements were performed using the measurement setup shown in Fig. 12. The results are depicted in Fig. 12, where the modulation can be easily observed for all the coverage angles. It can be seen that the measured signals include both the carrier frequency and modulation upper and lower sidebands. It should be noted that the measurements are normalized by the carrier frequency, f_c, of the RF generated by the signal generator. The carrier frequency f_c corresponds to a specific DoA as explained in Section II and presented in Fig. 3. In Fig. 12 (a) – (b) f_c is 24 GHz, and in Fig. 12 (c) – (d) f_c is 31 GHz, corresponding to a DoA of $-20°$ and $+10°$, respectively. From the results, it can be observed that the carrier frequency, f_c and the modulation sidebands ($f_c - f_m$ and $f_c + f_m$) of the measured received signal, both the 10 kHz and 20 kHz modulation frequencies (f_m) can be detected. Sideband suppression is between 10 dB and 20 dB. Thus, beam steering as well as detection capabilities were verified. Therefore, the BMT can receive, modulate, and reflect the signals transmitted by the LWA for the whole range of coverage angles. To be able to estimate DoA, distance and ID, the FMCW system presented in Section III should be employed.

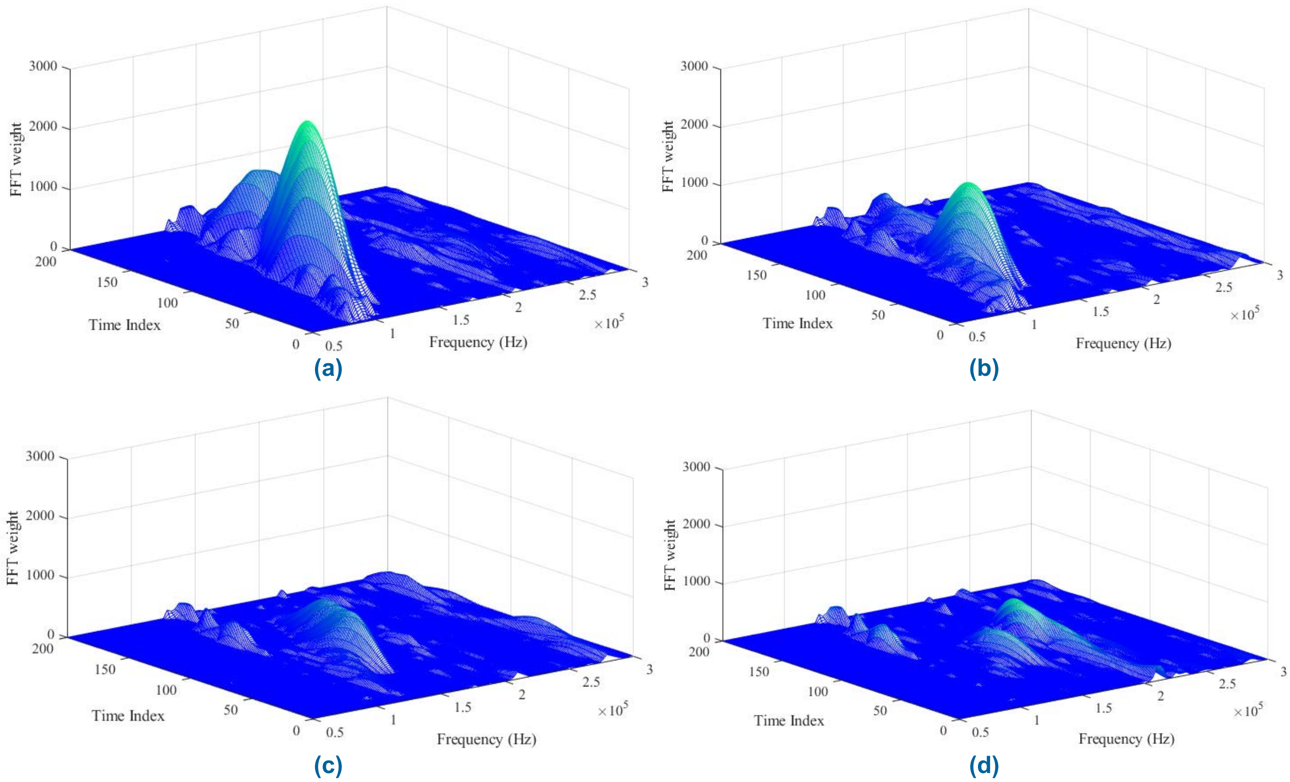

FIGURE 13. Sliding Hanning window FFT of the measured LWA FMCW radar echo at (a) 25 cm, (b) 50 cm (c) 75 cm and (d) 100 cm.

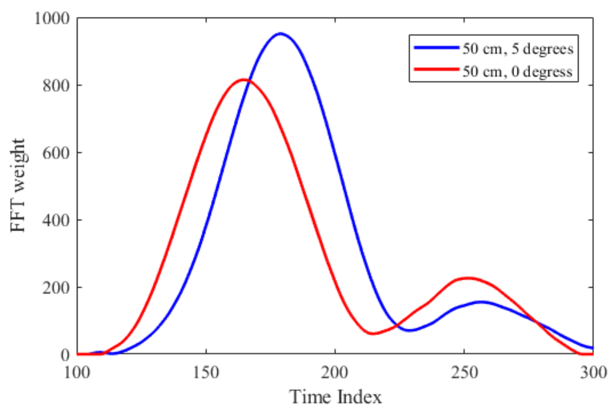

FIGURE 14. DoA measurements of the BMT at a distance of 50 cm and at an angle of (a) 0 degrees (red line), and (b) 5 degrees (blue line).

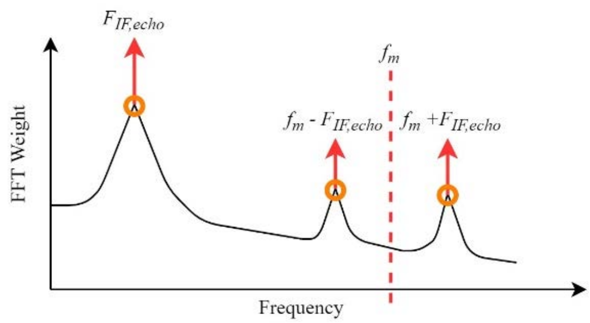

FIGURE 15. Received radar echoes of the BMTs ($F_{IF,echo}$) and its modulation signals (f_m).

The experimental setup of both the FMCW radar system and the BMT is shown in Fig. 7. Again, numerous measurements were carried out at different DoAs, distances and modulation frequencies. An oscilloscope was used to measure the downconverted (IF) FMCW radar signal. By processing the IF signal the target's echo was obtained. Fig. 13 shows the 3D plots of the FFT over time, obtained via a Hanning window of the measured IF waveforms. Using Equation (8) and the parameters of the proof-of-concept radar system, the maximum achievable distance is 200 cm. The measurements were for BMT ranges of 25, 50 and 75 and 100 cm. It can be seen that the BMT is detectable in all cases. The range between the radar and the BMT, R, can be estimated using the following expression, which is derived from (2) and (3):

$$R = \frac{c f_{\mathrm{IF,echo}}}{2\frac{B}{T}} \tag{9}$$

where, R is the range between the radar and the reflecting object, c is the speed of light, $f_{\mathrm{IF,echo}}$ is the measured frequency of the echo and B/T is the frequency change per unit of time. The frequencies of the measured echoes were at 125 kHz, 141 kHz, 160 kHz and 180.5 kHz, respectively. To correctly calculate the distance of the detected object, the length of the cables used by the radar system has to

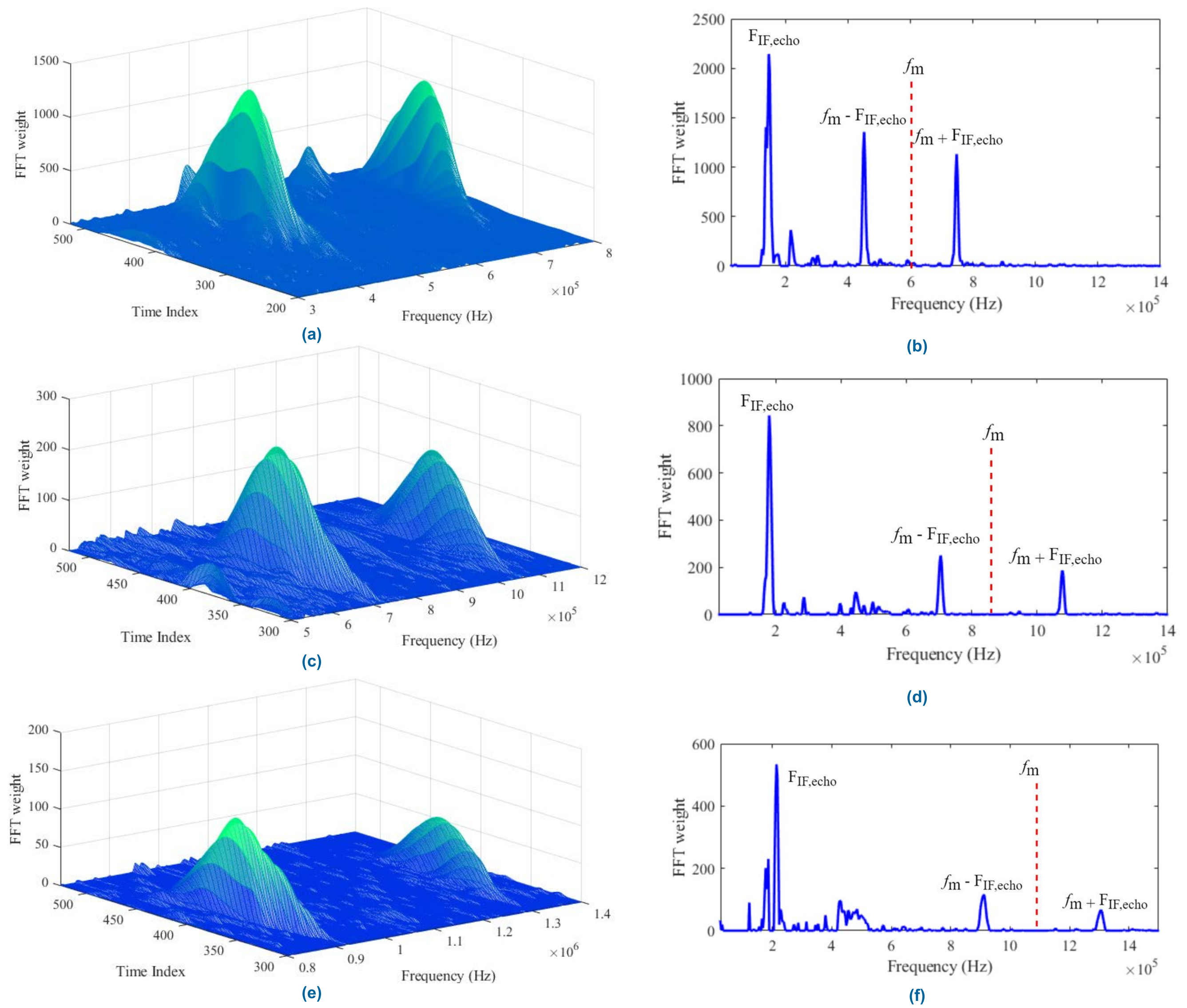

FIGURE 16. Sliding Hanning window FFT and spectrum at DoA of the measured LWA FMCW backscattering echoes with the following settings: (a) – (b) 25 cm and modulation frequency 600 KHz, (c) – (d) 50 cm and modulation frequency 900 KHz and (e) – (f) 100 cm and modulation frequency 1100 KHz.

be subtracted by the resulting range given by Equation (9). After doing this, the estimated range of the radar system was 25.7 cm, 49.7 cm, 78.2 cm, and 108 cm. These results were very close to the setup ranges of the BMTs with a measurement error below 8%. This shows that the FMCW radar can correctly detect the distance to the BMTs, which is the first step for the localization process.

In addition to the ranging of the BMTs, the FMCW radar can also detect the DoA of the BMTs. This achieved by plotting the FFT weights over the time index axis from the sliding window function. The DoA information is found via the 'Time Index' axis directly if the bandwidth and periodicity of the FMCW signal and the beam scanning behavior of the LWAs (shown in Fig. 3) are known. These three parameters are crucial in estimating the DoA of the BMTs based on the Time Index of their echo within the received IF waveform. The impact of the DoA on the radar echo along the Time Index axis can be seen in Fig. 14, where the echo of the BMT is shifted along the Time Index axis. This is because the DoA is different between the two measurements. In the first measurement (red line) the direction of arrival is 0° and in the second measurement (blue line) it is $+5^\circ$. As described above, the Time Index indicates the DoA of the BMTs. Here it can be seen that the Time Index for the echo of the first measurement (red line) is 160, and for the echo of the second measurement (blue line) it is 185. In this specific measurement, the antenna was steered from -30° to $+18^\circ$, the bandwidth of the FMCW signal was 10 GHz (23 to 33 GHz) and the periodicity was 250 ms. Based on these, the Time Index axis can be used to calculate the DoA.

Each Time Index point of the sliding window is directly related to a specific frequency point and radiation angle. For example, the whole BW is covered from Time Index 0 to 250 ($-30°$ to $18°$).

Additional measurements were performed to evaluate the third detection parameter of the BMTs, which is the backscattering modulation. As described above, the backscattering modulation can be used to identify the BMTs by detecting the introduced PM signal. The backscattering modulation can operate from a few kHz to a few MHz. Here, the modulation frequencies are chosen to be at least one order of magnitude higher than the highest expected radar IFs, to differentiate them rapidly and simply.

Due to the high modulated frequencies, the modulation sidebands of the PM will be seen by the FMCW radar at higher frequencies than the echoes of the BMTs. This is shown in Fig. 15 where the two modulation sidebands of the PM signal are located at $f_m - F_{IF,echo}$ and $f_m + F_{IF,echo}$. The modulation peaks are the modulation sidebands of the received signal and are located around the modulation frequency due to the mixing that is included in the FMCW signal. The frequency spacing between the modulation sidebands is twice the beat frequency of the target. Hence, the modulation sidebands can be used to localize and identify the BMTs by mixing at the modulation frequency, f_m. Fig. 16 shows the modulation sidebands of different PM frequencies received by the FMCW radar. Figs. 16 (a) – (b) show the Hanning window FFT of the IF waveform for a BMT at a distance of 25 cm and modulation frequency of 600 kHz. On the other hand, Figs. 16 (c) – (d) show the Hanning window FFT of the IF waveform for a BMT at a distance of 50 cm and modulation frequency of 900 kHz. Finally, Figs. 16 (e) – (f) show the Hanning window FFT of the IF waveform for a BMT at a distance of 100 cm and modulation frequency of 1.1 MHz. It can be seen that there are two modulation sidebands around the PM frequency ($f_\mathrm{m} - \mathrm{F}_{\mathrm{IF,echo}}$ and $f_\mathrm{m} + \mathrm{F}_{\mathrm{IF,echo}}$). As the distance increases, the spacing between the two sidebands increases since it is double the echo of the BMT ($\mathrm{F}_{\mathrm{IF,echo}}$), and as the frequency of the modulation (f_m) increases these two sidebands are varied accordingly. This change can be seen from the measurements depicted in Fig. 16, where the distance is progressively increasing. Additionally, the modulation sidebands are located at a lower noise floor since they are at higher frequencies. This is a clear advantage of implementing high frequency backscattering modulation at the targets, since it can push the target echoes to higher frequencies where the noise floor is lower, while still being able to determine its distance, DoA and identity. Additionally, this property of the presented radar system will result in a significant reduction of false alarms caused by unwanted targets located within the radar range. This is because the power spectral density is inversely proportional to the frequency of the signal (*1/f*). This could be beneficial not only for target identification but also for target detection and it can provide a significant advantage when dealing with high detection ranges. Furthermore, the location of the two modulation sidebands along the Time Index is again defined by the DoA. Hence, the Time Index of the modulation sidebands can be used in the same manner with the echo of the BMT to determine the DoA. Therefore, by capturing only the modulation sidebands, this is enough to localize and identify the BMTs. Finally, localization and identification is achieved using a single transceiver, providing a clear benefit since current state-of-the-art solutions such as UWB and WiFi localization systems require at least three transceivers.

VII. CONCLUSION

A novel photonically-enabled FMCW radar capable of localizing and identifying mobile terminals has been presented. The FMCW radar system uses a single transceiver with mm-wave LWAs to localize the detected mobile terminals. This is achieved by the beam scanning property of the two LWAs implemented. Additionally, backscattering technology has been employed in order to transfer information from the targets to the radar. To do so, an SPST switch was implemented at the antenna port of the mobile terminal. The backscattering mobile terminal is able to receive, modulate and backscatter the phase modulated RF. The FMCW radar receives the phase modulated echo of the backscattering mobile terminal and is able to localize it and identify it simultaneously. Several measurements have been presented using the proposed radar system to successfully localize and identify the BMTs. The calculation of the distance, direction-of-arrival and backscattered modulation frequency from the measurements has been demonstrated. In addition, localization and identification of BMTs at distances of up to 1 m has been demonstrated using backscattering modulation that decreases the influence and false alarms caused by the low-frequency noise. Finally, future work will be carried out to achieve 3D localization and identification.

REFERENCES

[1] D. Jiang and G. Liu, "An overview of 5G requirements," in *5G Mobile Communications*, 1st ed. New York, NY, USA: Springer, 2016.

[2] J. G. Andrews, S. Buzzi, W. Choi, S. V. Hanly, A. Lozano, A. C. K. Soong, and J. C. Zhang, "What will 5G be?" *IEEE J. Sel. Areas Commun.*, vol. 32, no. 6, pp. 1065–1082, Jun. 2014.

[3] A. Gupta and R. K. Jha, "A survey of 5G network: Architecture and emerging technologies," *IEEE Access*, vol. 3, pp. 1206–1232, 2015.

[4] L. Marnat, L. Dussopt, V. Puyal, A. Siligaris, F. Hameau, A. Larie, and C. Dehos, "V-band transceiver modules with integrated antennas and phased arrays for mmWave access in 5G mobile networks," in *Proc. 11th Eur. Conf. Antennas Propag. (EUCAP)*, Paris, France, Mar. 2017, pp. 2786–2790.

[5] A. A. Oliner and D. R. Jackson, "Leaky-wave antennas," in *Antenna Engineering Handbook*, 4th ed. New York, NY, USA: McGraw-Hill, 2007.

[6] U. Habib, M. Steeg, A. Stöhr, and N. J. Gomes, "Radio-over-fiber-supported millimeter-wave multiuser transmission with low-complexity antenna units," in *Proc. Int. Top. Meeting Microw. Photon. (MWP)*, Toulouse, France, Oct. 2018, pp. 1–4.

[7] S. Shahsavari, M. A. A. Khojastepour, and E. Erkip, "Robust beam tracking and data communication in millimeter wave mobile networks," in *Proc. Int. Symp. Modeling Optim. Mobile, Ad Hoc, Wireless Netw. (WiOPT)*, Avignon, France, Jun. 2019, pp. 1–8.

[8] F. Wen, H. Wymeersch, B. Peng, W. P. Tay, H. C. So, and D. Yang, "A survey on 5G massive MIMO localization," *Digit. Signal Process.*, vol. 94, pp. 21–28, Nov. 2019.

[9] O. Kanhere and T. S. Rappaport, "Position location for futuristic cellular communications: 5G and beyond," *IEEE Commun. Mag.*, vol. 59, no. 1, pp. 70–75, Jan. 2021.

[10] L. Qiu, X. Liang, and Z. Huang, "PATL: A RFID tag localization based on phased array antenna," *Sci. Rep.*, vol. 7, no. 1, Apr. 2017, Art. no. 44183.

[11] Z. Peng, L. Ran, and C. Li, "A *K*-band portable FMCW radar with beamforming array for short-range localization and vital-Doppler targets discrimination," *IEEE Trans. Microw. Theory Techn.*, vol. 65, no. 9, pp. 3443–3452, Sep. 2017.

[12] C. Loyez, M. Bocquet, and K. Haddadi, "Six-port technology for 5G millimeter-wave localization systems," in *Proc. Int. Conf. Electromagn. Adv. Appl. (ICEAA)*, Cartagena, Colombia, Sep. 2018, pp. 272–275.

[13] W. Y. Al-Rashdan and A. Tahat, "A comparative performance evaluation of machine learning algorithms for fingerprinting based localization in DM-MIMO wireless systems relying on big data techniques," *IEEE Access*, vol. 8, pp. 109522–109534, 2020.

[14] N. Xu, S. Li, C. S. Charollais, A. Burg, and A. Schumacher, "Machine learning based outdoor localization using the RSSI of multibeam antennas," in *Proc. IEEE Workshop Signal Process. Syst. (SiPS)*, Coimbra, Portugal, Oct. 2020, pp. 1–5.

[15] A. Costanzo, D. Dardari, J. Aleksandravicius, N. Decarli, M. D. Prete, D. Fabbri, M. Fantuzzi, A. Guerra, D. Masotti, M. Pizzotti, and A. Romani, "Energy autonomous UWB localization," *IEEE J. Radio Freq. Identificat.*, vol. 1, no. 3, pp. 228–244, Sep. 2017, doi: 10.1109/JRFID.2018.2792538.

[16] C. Laoudias, A. Moreira, S. Kim, S. Lee, L. Wirola, and C. Fischione, "A survey of enabling technologies for network localization, tracking, and navigation," *IEEE Commun. Surveys Tuts.*, vol. 20, no. 4, pp. 3607–3644, 4th Quart., 2018.

[17] L. Zwirello, T. Schipper, M. Harter, and T. Zwick, "UWB localization system for indoor applications: Concept, realization and analysis," *J. Electr. Comput. Eng.*, vol. 2012, pp. 1–11, 2012.

[18] M. Steeg, J. Tebart, K. Neophytou, M. A. Antoniades, S. Iezekiel, and A. Stöhr, "3D radar localization via photonic chirp leaky-wave antenna beam scanning," in *Proc. Int. Top. Meeting Microw. Photon. (MWP)*, Ottawa, ON, Canada, Oct. 2019, pp. 1–4.

[19] C.-H. Tseng and C.-H. Chao, "Noncontact vital-sign radar sensor using metamaterial-based scanning leaky-wave antenna," in *IEEE MTT-S Int. Microw. Symp. Dig.*, San Francisco, CA, USA, May 2016, pp. 1–3.

[20] K. Y. Kapusuz, A. V. Berghe, S. Lemey, and H. Rogier, "Partially filled half-mode substrate integrated waveguide leaky-wave antenna for 24 GHz automotive radar," *IEEE Antennas Wireless Propag. Lett.*, vol. 20, no. 1, pp. 33–37, Jan. 2021.

[21] V. Liu, A. Parks, V. Talla, S. Gollakota, D. Wetherall, and J. R. Smith, "Ambient backscatter: Wireless communication out of thin air," *SIGCOMM Comput. Commun. Rev.*, vol. 43, no. 4, pp. 39–50, Sep. 2013.

[22] J. Landt, "The history of RFID," *IEEE Potentials*, vol. 24, no. 4, pp. 8–11, Oct./Nov. 2005.

[23] V. Coskun, B. Ozdenizci, and K. Ok, "A survey on near field communication (NFC) technology," *Wireless Pers. Commun.*, vol. 71, no. 3, pp. 2259–2294, 2013.

[24] D. R. Jackson, C. Caloz, and T. Itoh, "Leaky-wave antennas," *Proc. IEEE*, vol. 100, no. 7, pp. 2194–2206, Jul. 2012.

[25] F. Monticone and A. Alù, "Leaky-wave theory, techniques, and applications: From microwaves to visible frequencies," *Proc. IEEE*, vol. 103, no. 5, pp. 793–821, May 2015.

[26] A. A. Oliner and D. R. Jackson, "Leaky-wave antennas," in *Antenna Engineering Handbook*, 4th ed. New York, NY, USA: McGraw-Hill, 2007.

[27] S. Otto and C. Caloz, "Importance of transversal and longitudinal symmetry/asymmetry in the fundamental properties of periodic leaky-wave antennas," in *Proc. IEEE Antennas Propag. Soc. Int. Symp. (APSURSI)*, Orlando, FL, USA, Jul. 2013, pp. 240–241.

[28] S. Paulotto, P. Baccarelli, F. Frezza, and D. R. Jackson, "A novel technique for open-stopband suppression in 1-D periodic printed leaky wave antennas," *IEEE Trans. Antennas Propag.*, vol. 57, no. 7, pp. 1894–1906, Jul. 2009.

[29] J. Liu, W. Zhou, and Y. Long, "A simple technique for open-stopband suppression in periodic leaky-wave antennas using two nonidentical elements per unit cell," *IEEE Trans. Antennas Propag.*, vol. 66, no. 6, pp. 2741–2751, Jun. 2018.

[30] P. Baccarelli, P. Burghignoli, D. Comite, W. Fuscaldo, and A. Galli, "Open-stopband suppression via double asymmetric discontinuities in 1-D periodic 2-D leaky-wave structures," *IEEE Antennas Wireless Propag. Lett.*, vol. 18, no. 10, pp. 2066–2070, Oct. 2019.

[31] G. V. Eleftheriades, "A generalized negative-refractive-index transmission-line (NRI-TL) metamaterial for dual-band and quad-band applications," *IEEE Microw. Compon. Lett.*, vol. 17, no. 6, pp. 415–417, Jun. 2007.

[32] S. Otto, A. Rennings, K. Solbach, and C. Caloz, "Transmission line modeling and asymptotic formulas for periodic leaky-wave antennas scanning through broadside," *IEEE Trans. Antennas Propag.*, vol. 59, no. 10, pp. 3695–3709, Oct. 2011.

[33] K. Neophytou, S. Iezekiel, M. Steeg, and A. Stöhr, "Design of PCB leaky-wave antennas for wide angle beam steering," in *Proc. 11th German Microw. Conf. (GeMiC)*, Freiburg, Germany, Mar. 2018, pp. 152–155.

[34] A. G. Stove, "Modern FMCW radar—Techniques and applications," in *Proc. 1st Eur. Radar Conf. (EURAD)*, Amsterdam, The Netherlands, 2004, pp. 149–152.

[35] J. Lee, Y.-A. Li, M.-H. Hung, and S.-J. Huang, "A fully-integrated 77-GHz FMCW radar transceiver in 65-nm CMOS technology," *IEEE J. Solid-State Circuits*, vol. 45, no. 12, pp. 2746–2756, Dec. 2010.

[36] R. J. Doviak and D. S. Zrni, *Doppler Radar and Weather Observations*, 2nd ed. New York, NY, USA: Dover, 1993.

[37] J. D. Griffin and G. D. Durgin, "Complete link budgets for backscatter-radio and RFID systems," *IEEE Antennas Propag. Mag.*, vol. 51, no. 2, pp. 11–25, Apr. 2009.

[38] P. Pursula, T. Vaha-Heikkila, A. Müller, D. Neculoiu, G. Konstantinidis, A. Oja, and J. Tuovinen, "Millimeter-wave Identification—A new short-range radio system for low-power high data-rate applications," *IEEE Trans. Microw. Theory Techn.*, vol. 56, no. 10, pp. 2221–2228, Oct. 2008.

[39] N. Van Huynh, D. T. Hoang, X. Lu, D. Niyato, P. Wang, and D. I. Kim, "Ambient backscatter communications: A contemporary survey," *IEEE Commun. Surveys Tuts.*, vol. 20, no. 4, pp. 2889–2922, 4th Quart., 2018.

[40] J. Kimionis, A. Georgiadis, and M. M. Tentzeris, "Millimeter-wave backscatter: A quantum leap for gigabit communication, RF sensing, and wearables," in *IEEE MTT-S Int. Microw. Symp. Dig.*, Jun. 2017, pp. 812–815.

[41] S. J. Thomas, E. Wheeler, J. Teizer, and M. S. Reynolds, "Quadrature amplitude modulated backscatter in passive and semipassive UHF RFID systems," *IEEE Trans. Microw. Theory Techn.*, vol. 60, no. 4, pp. 1175–1182, Apr. 2012.

[42] MACOM. *MADP-000907-14020P*. Accessed: Jan. 31, 2022. [Online]. Available: https://www.macom.com/products/product-detail/MADP-000907-14020P

KYRIAKOS NEOPHYTOU (Student Member, IEEE) received the B.Sc. degree in electrical and computer engineering from the University of Cyprus, Nicosia, Cyprus, in 2017, where he is currently pursuing the Ph.D. degree.

His research interests include leaky-wave antennas, metamaterials, RFID tags, microwave photonics, and wireless power transfer.

MATTHIAS STEEG (Member, IEEE) received the B.Sc. and M.Sc. degrees in electrical engineering and information technology and the Ph.D. degree from the University of Duisburg-Essen, Germany, in 2012, 2015, and 2021, respectively. He joined the Department of Optoelectronics, University of Duisburg-Essen, in 2015, as a Research Scientist working on photonic beam steering via leaky-wave antennas for mm-wave communication and radar. He is currently working as a Research and Development Manager at Muegge GmbH developing magnetron and solid-state-based high power microwave systems. His research interests include microwave and mm-wave wireless applications, fiber and mobile networks, and beam steering antennas.

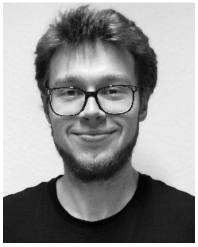

JONAS TEBART (Student Member, IEEE) received the B.Sc. and M.Sc. degrees in electrical engineering and information technology from the University of Duisburg-Essen, Duisburg, Germany, in 2016 and 2019, respectively, where he is currently pursuing the Ph.D. degree under the supervision of Prof. Andreas Stöhr.

After his studies with focus on microelectronics and optoelectronics, he joined the Department of Optoelectronics, University of Duisburg-Essen, as a Research Assistant. His research interests include radio-over-fiber (RoF) techniques, millimeter-wave (mm-wave) and THz communications, 5G, B5G and 6G mobile networks, photonic radars, as well as mm-wave beam-steering antennas.

ANDREAS STÖHR (Senior Member, IEEE) received the Dipl.-Ing. and Dr.-Ing. degrees in electrical engineering from Gerhard-Mercator-University, Duisburg, Germany, in 1991 and 1997, respectively.

From 1987 to 1996, he was the CEO of MS Steuerungsanlagen GmbH, Germany. From 1996 to 2013, he was a Research Scientist with the University of Duisburg-Essen (UDE), Duisburg. During that period, in 1998 and 1999, he also joined the Communications Research Laboratory (CRL), Tokyo, Japan, where he worked on 60 GHz wireless systems employing radio over fiber techniques. He was also with France Telecom Orange Labs, Lannion, France, in 2009; and Corning, in 2015. Since 2011, he has been a Professor and the Head of the Center for Semiconductor Technology and Optoelectronics (ZHO), Optoelectronics Department, UDE. He is currently a Visiting Professor with the University of Ottawa, Ottawa, ON, Canada. He has authored or coauthored more than 200 papers in refereed journals and conferences. His current research interests include III/V integrated microwave photonic device technology and RF photonic integration technologies for millimeter-wave and THz communications, measurement systems, as well as sensing applications. He is a Senior Member of the IEEE Photonics and MTT Society, a committee member and the chair of a number of international conferences, and a guest editor of IEEE/OSA.

STAVROS IEZEKIEL (Senior Member, IEEE) received the B.Eng. and Ph.D. degrees in electronic and electrical engineering from the University of Leeds, in 1987 and 1991, respectively.

From 1993 to 2006, he was on the Academic Staff at the University of Leeds, where he has worked as the Deputy Director of the Institute of Microwaves and Photonics and also as the Director of learning and teaching at the Department of Electronic and Electrical Engineering (in which role he launched a M.Eng. degree program in photonics that was funded by Agilent Technologies). From 2010 to 2014, he was the President of the Department of Electrical and Computer Engineering. In 2011, he was an Invited Professor at ESIEE Paris. He is currently a Professor at the University of Cyprus, where he leads the research activity in microwave photonics and space photonics (the latter with funding from the European Space Agency). He is the Director of the EMPHASIS Research Centre (an interdepartmental research center targeting electronics, microwaves, photonics, and sensing). He has published over 170 papers and edited a book in microwave photonics. His current research interests include integrated microwave photonics and photonic generation of microwaves with applications to high-throughput satellite payloads and 5G mm-wave radio-over-fiber.

Prof. Iezekiel is a Fellow of IET and the Institute of Physics. He has received the 1999 IEE/NPL Measurements Prize for his work in microwave photonic measurements. He is active within several professional societies, mostly the IEEE, where he has served on a number of different committees, guest-edited special issues, and organized or co-organized a number of high-profile events in microwaves and photonics. He has served as the Editor-in-Chief for *IET Microwaves, Antennas and Propagation*, from 2009 to 2019.

MARCO A. ANTONIADES (Senior Member, IEEE) received the B.A.Sc. degree in electrical engineering from the University of Waterloo, ON, Canada, in 2001, and the M.A.Sc. and Ph.D. degrees in electrical engineering from the University of Toronto, ON, Canada, in 2003 and 2009, respectively.

His research interests include engineered electromagnetic materials (metamaterials, metasurfaces), electrically-small antennas, adaptive and reconfigurable antennas, RF/microwave circuits and devices, implantable/wearable antennas, microwave imaging, wireless power transfer, and radio-frequency identification. He is a member of the IEEE AP-S Education Committee and a member of the IEEE SIGHT Special Interest Group on Humanitarian Technology. He was a recipient of the Academic Excellence Award from the Hellenic Canadian Federation of Ontario, in 2003, the First Prize in the Student Paper Competition at the 2006 IEEE AP-S International Symposium on Antennas and Propagation (AP-S/URSI), the Best of IEEE Computer Architecture Letters Award, in 2018, and the Teaching Innovation Award from the University of Cyprus, in 2018. He has served as the Conference Chair for the 2015 Loughborough Antennas and Propagation Conference (LAPC), on the Steering Committee for the 2010 IEEE AP-S/URSI International Symposium, and as a Co-Chair of the Technical Program Committee for the 2020 IEEE AP-S/URSI International Symposium. He has served as an Associate Editor for *IET Microwaves, Antennas and Propagation*, from 2014 to 2018. He is an Associate Editor of the IEEE Antennas and Wireless Propagation Letters and the IEEE Transactions on Antennas and Propagation.